5-1999

Neutron Resonance Spectroscopy of 117Sn from1 eV to 1.5 keV

D A. Smith
Los Alamos National Laboratory

J D. Bowman
Los Alamos National Laboratory

Bret E. Crawford
Gettysburg College

See next page for additional authors

Smith, D. A., Bowman, J. D., Crawford, B. E., Grossmann, C. A., Haseyama, T., Johnson, M. B., Masaike, A., Masuda, Y., Mitchell, G. E., Nazarenko, V. A., Penttila, S.I., Roberson, N. R., Seestrom, S. J., Sharapov, E I., Smotritsky, L. M., Stephenson, S., & Yuan, V. W. (1999) Neutron Resonance Spectroscopy of 117Sn from1 eV to 1.5 keV. Physical Review C, 59(5), 2836–2843. http://dx.doi.org/10.1103/PhysRevC.59.2836

Neutron Resonance Spectroscopy of 117Sn from1 eV to 1.5 keV

Abstract

Parity violation has been studied recently for neutron resonances in ^{117}Sn. The neutron resonance spectroscopy is essential for the analysis of the parity violation data. We have measured neutron resonances in ^{117}Sn for neutron energies from 1 to 1500 eV using the time-of-flight method and the (n,γ) reaction. The sample was enriched to 87.6% ^{117}Sn. Neutron scattering and radiative widths were determined, and orbital angular momentum assignments were made with a Bayesian analysis. The s-wave and p-wave strength functions and average level spacings were determined.

Disciplines

Atomic, Molecular and Optical Physics | Physics

Authors

D A. Smith, J D. Bowman, Bret E. Crawford, C A. Grossmann, T Haseyama, Mikkel B. Johnson, A Masaike, Y Matsuda, G E. Mitchell, V A. Nazarenko, S I. Penttila, N R. Roberson, S J. Seestrom, E I. Sharapov, L M. Smotritsky, Sharon L. Stephenson, and V W. Yuan

Neutron resonance spectroscopy of ^{117}Sn from 1 eV to 1.5 keV

D. A. Smith,[1] J. D. Bowman,[1] B. E. Crawford,[2,*] C. A. Grossmann,[3] T. Haseyama,[4] Mikkel B. Johnson,[1] A. Masaike,[4] Y. Matsuda,[4,†] G. E. Mitchell,[3] V. A. Nazarenko,[5] S. I. Penttila,[1] N. R. Roberson,[2] S. J. Seestrom,[1] E. I. Sharapov,[6] L. M. Smotritsky,[5] S. L. Stephenson,[3,‡] and V. Yuan[1]

[1]*Los Alamos National Laboratory, Los Alamos, New Mexico 87545*

[2]*Duke University, Durham, North Carolina 27708*
and Triangle Universities Nuclear Laboratory, Durham, North Carolina 27708-0308

[3]*North Carolina State University, Raleigh, North Carolina 27695-8202*
and Triangle Universities Nuclear Laboratory, Durham, North Carolina 27708-0308

[4]*Physics Department, Kyoto University, Kyoto 606-01, Japan*

[5]*Petersburg Nuclear Physics Institute, 188350 Gatchina, Russia*

[6]*Joint Institute for Nuclear Research, 141980 Dubna, Russia*

(Received 21 October 1998)

Parity violation has been studied recently for neutron resonances in ^{117}Sn. The neutron resonance spectroscopy is essential for the analysis of the parity violation data. We have measured neutron resonances in ^{117}Sn for neutron energies from 1 to 1500 eV using the time-of-flight method and the (n,γ) reaction. The sample was enriched to 87.6% ^{117}Sn. Neutron scattering and radiative widths were determined, and orbital angular momentum assignments were made with a Bayesian analysis. The *s*-wave and *p*-wave strength functions and average level spacings were determined. [S0556-2813(99)04403-9]

PACS number(s): 25.40.Ny, 24.80.+y, 11.30.Er, 27.60.+j

I. INTRODUCTION

After the discovery of a large enhancement of parity violation for neutron resonances in heavy nuclei [1], a new approach was adopted to the study of symmetry breaking. The symmetry-breaking matrix elements are treated as random variables, and the experimental goal is the measurement of the root-mean-square symmetry-breaking matrix element. This new approach to nuclear parity nonconservation (PNC) is discussed in recent reviews [2,3]. The early experiments were limited in both energy range and in sensitivity. The TRIPLE Collaboration measured many parity violations in ^{238}U and ^{232}Th and determined rms PNC matrix elements [4,5]. These measurements were in the vicinity of the $4p$ neutron strength function maximum. To determine the mass dependence of the effective weak nucleon-nucleus interaction, PNC measurements are required in other mass regions. Our focus has been on $A \simeq 100$, the region of the $3p$ neutron strength function maximum. The mean-squared magnitude of the PNC effects is proportional to the level density, and the average level density is smaller for the lower mass $A \simeq 100$ nuclei than for the $A \simeq 230$ nuclei. From this point of view, it is preferable in the $A \approx 100$ region to study odd-mass targets with their higher level density. However, in order to extract the rms PNC matrix element from the data, neutron resonance parameters are required for both the *s*-wave and *p*-wave resonances [6]. Thus a prerequisite for the PNC analysis is knowledge of the relevant neutron resonance spectroscopy.

Our group had access to an enriched ^{117}Sn target, which seemed an excellent candidate for PNC measurements. The ^{117}Sn nucleus has some special features that made the study of parity violation interesting. First, the ^{118}Sn daughter has a closed shell of protons. The excitations near the neutron separation energy are overwhelmingly made up of couplings of multiparticle-multihole valence neutron configurations. The matrix elements of the two-body parity-violating part of the $\Delta I = 1$ pion-nucleon exchange potential vanish. Second, there are no one-body matrix elements of the weak force associated with deformation since ^{118}Sn is spherical. In practice a number of parity violations were observed in ^{117}Sn [7]. However, in order to analyze the parity violation data, an improved understanding of the neutron resonance spectroscopy was required. The earlier experiments provided relatively little information on most of the weaker *p*-wave resonances, and the resonance parameters were poorly determined [8]. With the high epithermal neutron flux available at the Manuel Lujan Neutron Scattering Center at the Los Alamos Neutron Scattering Center (LANSCE), we were able to improve significantly the neutron resonance spectroscopy of ^{117}Sn.

In Sec. II the experimental procedure is described. The analysis to determine the resonance parameters is presented in Sec. III. The orbital angular momenta, strength functions, and level densities are discussed in Sec. IV. Results of statistical tests to evaluate the data quality are presented in Sec. V. The final section provides a brief summary.

II. EXPERIMENTAL PROCEDURE

The data were measured at flight path 2 of LANSCE, where neutrons are created by the spallation process from an

*Present address: North Carolina State University, Raleigh, NC 27695-8202 and Gettysburg College, Gettysburg, PA 17325.

†Present address: Institute of Physical and Chemical Research (RIKEN), Saitama, 351-0198, Japan.

‡Present address: Gettysburg College, Gettysburg, PA 17325.

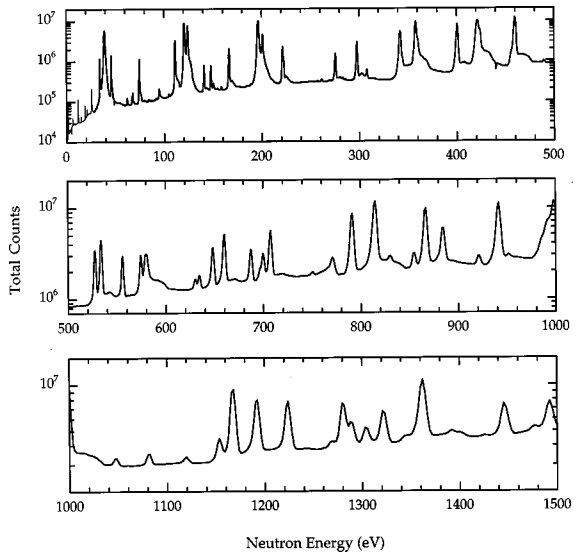

FIG. 1. Neutron time-of-flight spectrum for ^{117}Sn. The spectrum from 1 to 30 eV has been relatively normalized to the data from 30 to 1500 eV, and plotted here on the same scale.

800 MeV proton pulse onto a tungsten target, and are moderated down to low energies using chilled water [9]. The neutron energy was determined from the time of flight over a 59.4-m distance from source to detector. The detector is an array of 24 CsI crystals with approximately 3.5π of detection solid angle. The crystals are packed tightly around the target in two arrays of 12 crystals each, with a 10-cm cylindrical hole through the middle to allow access for the neutron beam [10]. The scintillation light from the CsI crystals is detected by photomultiplier tubes (PMT's). The PMT signals are converted to logic pulses by constant fraction discriminators. In order to reduce the rate of the background signal, a coincidence of two signals from the detector was required for an event. The event pulses were counted by a multiscaler attached to an averaging memory. The start time of the multiscaler spectra is derived from the proton pulse. The multiscaler dwell time was set to 100 ns to cover a time-of-flight range of 0–0.8196 ms and to 1 μs in order to cover a time-of-flight range of 0–8.196 ms. The data was analyzed in the energy interval from 27 eV to 2.1 keV.

The target was an 87.6%-enriched ^{117}Sn solid metal target, in the form of a rectangle of 7.7 cm$\times$6.3 cm on average and 1.3 cm thick. Other nuclides in the target were the other stable tin isotopes, except for a 0.05% platinum impurity, which we assume came from the crucible used to manufacture the target. The target was placed in the center of the two CsI crystal arrays, where the normal to the 7.3 cm $\times$6.3 cm area of the target was along the beam direction. A typical spectrum measured in this experiment is shown in Fig. 1. The number of counts in each 0.1-μs and 1.0-μs time-of-flight bin is plotted versus neutron energy. On this plot the longer dwell time spectrum (events below 30 eV) has been normalized to the shorter dwell time spectrum.

III. RESONANCE STRENGTHS

The time-of-flight spectra were analyzed using the fitting code FITXS [11]. This code was developed for the analysis of neutron resonances, where the neutrons were created with a moderated pulsed neutron beam. The code can analyze resonances measured by neutron transmission or radiative capture. In the present work, we analyzed neutron resonances measured via radiative capture. The code includes all major resolution effects on the neutron time-of-flight spectra. Effects of moderation time, detector efficiencies, flight path length, target temperature, proton pulse width, etc., are incorporated in the code so that the resonance parameters (neutron energy, neutron width, and total gamma-ray width) can be determined directly from the data. Application of this analysis program is described in our recent papers [4,12].

A sample fit to a time-of-flight region is shown in Fig. 2. In the figure neutron counts per 0.1-μs time-of-flight bin are plotted versus time of flight, with the fit to the data shown as a solid curve. The main difficulties in the analysis are illustrated in this section of the data. There are three *p*-wave resonances in ^{117}Sn in this energy range, and also resonances from five other tin isotopes and two platinum isotopes, plus background. In order to determine the resonance parameters accurately for the ^{117}Sn resonances, resonances from other nuclides had to be fit along with the *p*-wave resonances of interest. In this section of the spectrum, additional capture peaks after multiple scattering are visible as broad bumps on the high-energy side of resonances. Multiple-scattering corrections will be discussed later in this section.

In the course of the PNC study, conditions were optimized for a high count rate. As a consequence, dead-time corrections are important. The detector count rate efficiency appeared to be different in resonance and background regions for the first 200 μs in the time-of-flight spectrum. We attribute this change to detector overloading in response to the prompt flash of γ rays and fast neutrons. Corrections were made by comparing the high count rate run with a run which was taken at one-tenth of the normal beam intensity. The maximum dead-time corrections for resonances were about 35%.

The true start of the time-of-flight spectrum was measured directly as the position of the prompt γ-ray peak in the spectrum obtained at a low beam intensity, yielding a time offset of 1.55 ± 0.05 μs. This offset was constant for all subsequent data; the error quoted here is one-half the multiscaler dwell time. The flight path length of 59.39 ± 0.02 m was determined by fitting peaks to known neutron resonance energies in samples of ^{103}Rh, ^{117}Sn, ^{127}I, and ^{232}Th [13], which were studied during the same run cycle. The ^{232}Th resonances provided the highest accuracy for this calibration [13,5]. The errors in determining the flight path length and time offset are the dominant systematic errors in the measured energies of the neutron resonances, where the statistical error of an energy measurement was about 0.001%.

In order to extract resonance parameters from the capture data, knowledge of the neutron flux and detector efficiency is required. These were obtained by fitting the detector count rate to known resonance parameters for many resonances in ^{117}Sn. However, several resonances were partially obscured by peaks from trace amounts of manganese and copper in the vacuum windows and other material in the beam. Corrections due to manganese of 40% and 5% were made to the 342-eV and 358-eV resonances, respectively. The copper contamination occurred at the same energy as the 580-eV

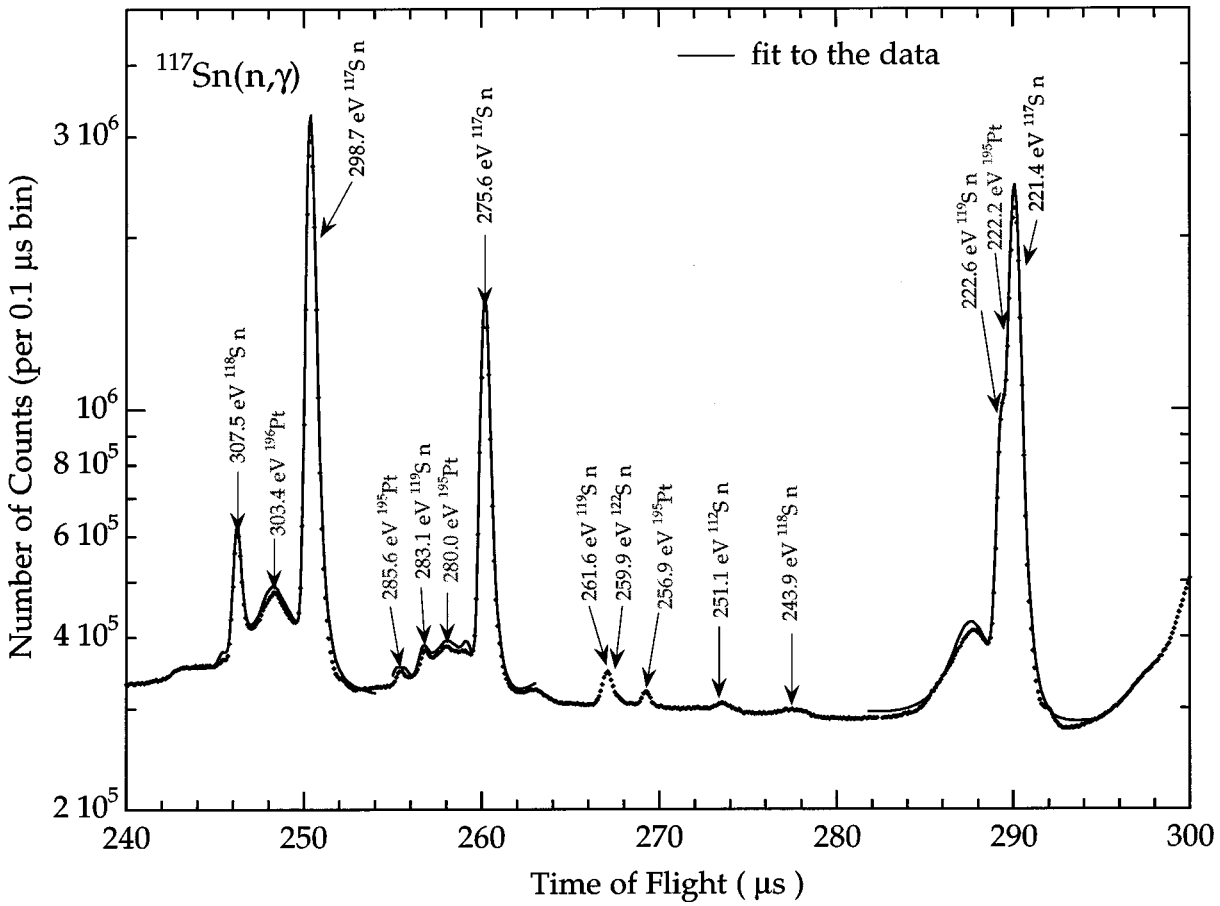

FIG. 2. Fit to a section of the time-of-flight spectrum. The data are plotted as points, and the fit obtained with the code FITXS is shown as a line.

resonance in ^{117}Sn and distorted this state beyond our ability to correct effectively. No resonance parameters could be determined for the 580-eV resonance, although the nearby 573.2-eV *p*-wave resonance was unaffected.

The energy dependence of the neutron flux is known to be a power law in neutron energy, $\Phi(E)=cE^{-\alpha}$ [14]. From fitting the data to known neutron resonance parameters, there was an 11% uncertainty in c and a 7% uncertainty in α, primarily determined by the accuracy of the resonance parameters in ^{117}Sn. To reduce the uncertainty in the flux calibration we used flux data from a ^{3}He scintillation detector, obtained on our flight path during that year with the same beam configuration [15]. The efficiency of this detector versus neutron energy is very well known, and the measurements with the ^{3}He scintillation detector provided an accurate determination of the power law exponent in the neutron flux: $\alpha=0.956\pm0.001$. The neutron flux could then be fit to the known ^{117}Sn data, yielding a final error of 5% in the neutron flux. We were concerned that there could be different detector efficiencies for *s*-wave and *p*-wave resonances. Therefore the normalization fitting was performed separately for *s*-wave and *p*-wave resonances. Within the 6% uncertainty, the analysis gave the same efficiency for the *s*-wave and *p*-wave resonances. The calibration uncertainty produces the dominant error in the measured neutron widths, since the statistical error was about 0.1%.

A major problem in the data analysis was the presence of neutron capture after multiple scattering in the sample. In our 13-mm-thick target, approximately 19% of incoming neutrons were scattered in the first interaction due to *s*-wave potential elastic scattering. Numerical estimates of the multiple-scattering contribution performed with a Monte Carlo code [16] gave typical values of 25% relative to the primary resonance capture. The neutron energy loss averaged over all scattering angles is $\Delta E\simeq 2E/A$, and neutrons with an energy $E=E_0+\Delta E$ higher than the resonance energy E_0 are effectively captured after scattering. Multiple scattering produces an additional peak or shoulder at the higher-energy side of a resonance in the time-of-flight spectrum depending on whether the ΔE value is larger or smaller than the resonance width (in our case, the widths were determined by the Doppler width below $E\simeq 200$ eV and the instrumental width above 200 eV). For most of the ^{117}Sn resonances below 1 keV, secondary peaks could be fitted separately from the resonance peaks and subtracted from the data. We used this procedure to correct for the multiple-scattering effects, except for the 38-eV *s*-wave resonance, where the distortions due to multiple scattering could not be effectively corrected and the resonance parameters could not be determined from these data.

Our results for the neutron resonance parameters are listed in Table I. For completeness, some results from earlier experiments [8,13] are also included. We identified 23 new resonances in ^{117}Sn up to 1500 eV. Most of these new resonances are *p*-wave resonances, which were not observed before because of lower neutron fluxes in eariler experiments.

TABLE I. Neutron resonance parameters for ^{117}Sn.

Energy (eV)	J	l	B.P.	$g\Gamma_n$ (meV)	Γ_γ (meV)	$g\Gamma_n^l$ (meV)	
−29.2		0				5.55	a
1.327±0.001		1	0.99	0.000138±0.000007	148±10	42.8±2.1	b
15.385±0.016		1	0.99	0.000092±0.000005	136±18	0.72±0.04	c
21.390±0.025		1	0.99	0.000206±0.000011	113±16	0.99±0.05	c
26.215±0.034		1	0.98	0.00207±0.00010	129±8	7.32±0.4	c
34.044±0.017		1	0.96	0.0187±0.0009	119±9	44.8±2.2	b
38.80±0.05	1	0	0.00	3.10±0.15	100±15	0.50±0.02	a
74.39±0.04		1	0.96	0.034±0.002		25.20±1.3	b
120.54±0.06	1	0	0.00	4.95±0.25	107±12	0.45±0.02	b
123.90±0.07	0	0	0.00	2.1±0.1		0.19±0.01	b
158.33±0.09		1	0.96	0.0025±0.0001		0.60±0.03	c
166.32±0.09		1	0.93	0.160±0.008		35.4±1.8	b
196.20±0.11	1	0	0.00	12.2±0.6	104±13	0.87±0.04	b
200.78±0.12		1	0.84	0.48±0.02		79.6±4.0	b
221.17±0.13		1	0.92	0.22±0.01		31.1±1.6	b
275.21±0.17		1	0.93	0.17±0.01		17.3±0.9	b
297.36±0.18		1	0.90	0.43±0.02		40.1±2.0	b
341.63±0.22		0	0.00	15.9±0.8		0.86±0.04	b
357.60±0.23		0	0.00	12.0±3.5		0.63±0.2	b
400.03±0.27		0	0.23	3.7±0.2	110±19	0.19±0.01	b
420.73±0.28	1	0	0.00	62.5±7.5	105±20	3.0±0.4	d
423.29±0.28		1	0.77	1.55±0.08		84.5±4.2	c
458.99±0.32	0	0	0.00	12.5±1.5		0.58±0.07	d
488.46±0.34		1	0.93	0.036±0.002		1.59±0.09	c
526.34±0.38		1	0.87	0.96±0.07		37.9±2.6	b
532.62±0.38		1	0.83	1.46±0.10		56.6±4.0	b
554.57±0.40		1	0.89	0.74±0.06		27.0±2.1	b
573.24±0.42		1	0.89	0.78±0.06		27.2±2.2	c
580.8±1.0	0	0	0.00	30±3		1.25±0.1	a
628.59±0.47		1	0.92	0.141±0.013		4.25±0.4	c
646.68±0.49		1	0.87	1.20±0.12		34.6±3.3	b
658.50±0.50		1	0.81	2.2±0.2		60.8±6.0	b
685.74±0.53		1	0.87	1.15±0.12		30.5±3.2	b
694.43±0.54		1	0.92	0.19±0.02		5.0±0.5	c
698.31±0.54		1	0.90	0.72±0.08		18.5±2.0	c
705.76±0.55		(0)	0.78	2.6±0.3		0.10±0.01	b
789.41±0.64		0	0.16	11.0±1.3		0.39±0.05	b
812.92±0.66	1	0	0.00	65±6	91±27	2.28±0.2	d
852.58±0.71		1	0.89	0.79±0.10		15.0±1.9	c
864.51±0.72		0	0.26	10.5±2.1		0.36±0.07	b
882.31±0.74		1	0.77	3.6±0.5		65.3±8.70	b
939.22±0.80		0	0.03	20±2		0.65±0.07	d
983.29±0.85		1	0.89	0.92±0.13		14.1±2.0	c
989.37±0.86		0	0.00	200±30		6.4±1.0	d
996.13±0.87		0	0.00	90±15		2.9±0.5	d
1044.97±0.93		1	0.90	0.42±0.06		5.9±0.9	c
1078.56±0.97		1	0.89	0.66±0.10		8.8±1.4	c
1116.5±1.0		1	0.90	0.37±0.06		4.7±0.7	c
1150.1±1.1		1	0.88	1.14±0.18		13.9±2.2	c
1164.5±1.1		0	0.27	15.6±2.5		0.46±0.07	b
1189.1±1.1		0	0.57	9.7±1.6		0.28±0.05	b
1220.7±1.1		0	0.62	8.8±1.5		0.25±0.04	b
1277.1±1.2		0	0.67	8.1±1.4		0.23±0.04	b
1285.0±1.2		1	0.85	2.3±0.4		23.9±4.1	c
1300.7±1.3		1	0.86	1.9±0.3		19.8±3.4	c

TABLE I. (*Continued*).

Energy (eV)	J	l	B.P.	$g\Gamma_n$ (meV)	Γ_γ (meV)	$g\Gamma_n^l$ (meV)	
1318.5±1.3		1	0.77	5.5±0.9		54.4±9.4	b
1342.3±1.3		1	0.89	0.35±0.06		3.4±0.6	b
1358.6±1.3	1	0	0.00	88±9	81±30	2.4±0.2	d
1388.7±1.4		1	0.88	0.80±0.14		7.4±1.3	c
1397.7±1.4		1	0.88	0.53±0.09		4.8±0.9	c
1442.0±1.4		1	0.74	7.3±1.3		63.5±11.45	b
1472.8±1.5		1	0.88	0.88±0.16		7.5±1.4	c
1488.5±1.5		0	0.00	74±7.5		1.91±0.2	d

[a]Resonance parameters from Ref. [13].
[b]New resonance parameters from this work.
[c]New resonance identified in this work.
[d]Only new energy from this work; other resonance parameters from Ref. [8].

With our longer flight path, we have determined resonance energies with uncertainties about 50% smaller than earlier work. For the majority of resonances the parameter $g\Gamma_n$ was determined using an average Γ_γ value obtained at low energy. For such cases there is no entry listed in Table I. The shape analysis of good-resolution low-energy data enabled the determination of the radiative widths for 12 resonances, of which five were *p*-wave resonances and seven were *s*-wave resonances. Average radiative widths for *s*-wave and *p*-wave resonances are listed in Table II; the uncertainties are the average of the errors on individual resonance widths. These values are consistent with the systematics of radiative widths [13].

We note that a single-target capture cross section measurement cannot provide precise determination of $g\Gamma_n$ when the neutron width is of the order of the radiative width or larger, unless the resonance spin is known as well as an accurate value of Γ_γ. Qualitatively this is clear from the equation for the limiting case of a thin sample:

$$\frac{1}{A_\gamma}=\frac{1}{(g\Gamma_n)}+\frac{1}{g\Gamma_\gamma}. \tag{1}$$

Here A_γ is the properly normalized capture area and g is the statistical factor:

$$g=\frac{(2J+1)}{(2i+1)(2I+1)}, \tag{2}$$

where J is the total spin of the *s*-wave resonance, I is the spin of the target nucleus, and i is the spin of the captured neutron. For small $g\Gamma_n$ values the first term dominates which allows the determination of $g\Gamma_n$ nearly independent of other parameters. On the other hand, for large $g\Gamma_n$ and reasonably well known Γ_γ, Eq. (1) can be used to determine g, and thus obtain J (for ^{117}Sn, $g=1/4$ for $J=0$, and $g=3/4$ for $J=1$). This was the case for the 812-eV resonance.

IV. ORBITAL ANGULAR MOMENTUM

After the neutron resonance parameters were determined, the probability that a resonance was *s* wave or *p* wave was estimated. The estimates were calculated with a Bayesian analysis developed by Bollinger and Thomas [17] with the use of the Porter-Thomas distribution as a probability density for the reduced neutron widths. Using the notation of Frankle *el al.* [18], the probability of a resonance being *p* wave is

$$P=\left\{1+\frac{4}{9}\sqrt{\frac{4S_1c^0(E)}{3S_0c^1(E)}}\times\exp\left[-\frac{g\Gamma_n c^0(E)}{2D_0}\left(\frac{1}{S_0}-\frac{3c^1(E)}{4S_1c^0(E)}\right)\right]\right\}^{-1}, \tag{3}$$

where S_0 and S_1 are the *s*-wave and *p*-wave strength functions, respectively, D_0 is the average *s*-wave level spacing, and Γ_n is the neutron width for the state. A resonance was assumed to be *p* wave if the probability P was greater than the *a priori* probability 69% and *s* wave if the probability was less than 69%. Of course the assignment is less reliable when the probability P is close to the *a priori* value. The functions $c^l(E)$ are

$$c^l(E)=\frac{[1+(kR)^{2l}]}{(kR)^{2l}\sqrt{E}} \tag{4}$$

and in the case of ^{117}Sn, for $l=0$ and 1,

TABLE II. Average radiative widths, level spacings, and strength functions for ^{117}Sn.

Values	$\langle\Gamma_{\gamma 0}\rangle$ (meV)	$\langle\Gamma_{\gamma 1}\rangle$ (meV)	D_0 (eV)	S_0 (10^{-4} eV)	S_1 (10^{-4} eV)
Current [a]	103±6	130±10	59.3±4.0	0.17±0.05	3.4±1.0
Previous [b]	80±20		48±6	0.21±0.04	3.0±1.6

[a]Values from this work.
[b]Values from Mughabghab *et al.* [13].

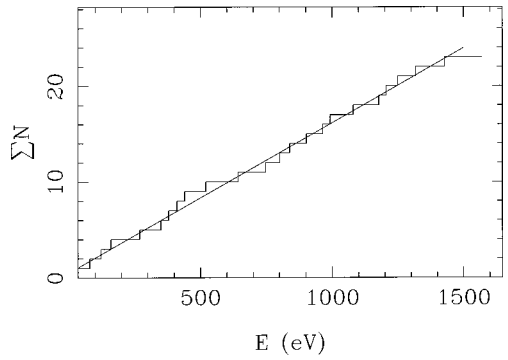

FIG. 3. Cumulative number of *s*-wave resonances. The line is a linear fit used to extract the *s*-wave level spacing.

$$c^0(E)=\frac{1}{\sqrt{E}} \quad \text{and} \quad c^1(E)=\frac{1}{\sqrt{E}}\left(\frac{4.75\times 10^5}{E}\right), \tag{5}$$

where the energy E is in eV and the nuclear radius is assumed to be $R=1.35A^{1/3}$ fm.

The probabilities depend on the *s*- and *p*-wave strength functions and the average *s*-wave level spacing. The strength functions were determined from the data in the usual way, by summing the reduced width over a range of energies,

$$S_l=\frac{1}{(2l+1)\Delta E}\sum g\Gamma_n^l, \tag{6}$$

and the reduced widths were calculated from

$$g\Gamma_n^l=c^l(E)g\Gamma_n. \tag{7}$$

The values for the strength functions change as the orbital angular momentum assignments are made. This process—of assigning resonances with this probabilistic argument, and then determining the strength functions and level densities—was iterated until the values stabilized. At the end, the values for the strength functions and level spacings were unchanged if one or two resonance assignments were changed. The final probabilities are listed in Table I under the column labeled B.P., along with the neutron resonance parameters. An exception was made for the 705.76-eV resonance which we assign $l=0$ to avoid a very large spacing (between the 580.8-eV and 789.4-eV resonances) in compliance with the Wigner distribution discussed in Sec. V.

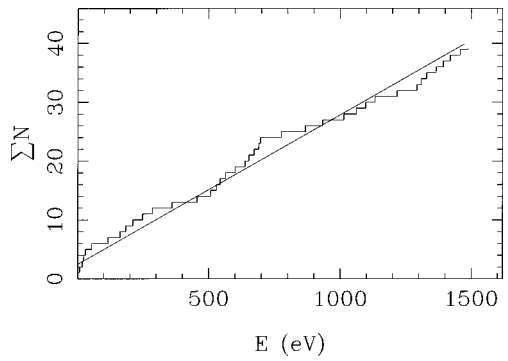

FIG. 4. Cumulative number of *p*-wave resonances. The line is a linear fit as discussed in Sec. V.

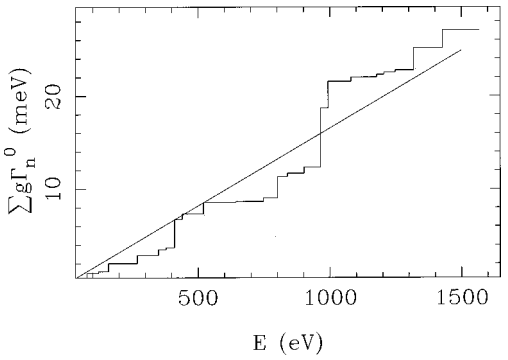

FIG. 5. Cumulative reduced neutron width for ^{117}Sn *s*-wave resonances with a linear fit used to extract the *s*-wave strength function.

From these assignments, plots of the cumulative number of states as a function of energy were prepared. These are shown in Figs. 3 and 4. Although both plots can be fit with a linear function, this does not ensure that all levels are observed in the experiment. To estimate the missing fraction of levels one must consider the distribution of neutron widths. This is discussed in the next section. After applying an 8% correction to the value of 64 eV extracted from the linear fit in Fig. 3 (see Sec. V for determination of missing fraction), we obtained the *s*-wave spacing $D_0=(59.3)\pm 4.0$ eV. Determining the *p*-wave average spacing is more involved. As a result of a large fraction of missing levels, the uncorrected value of 39.4 eV extracted from Fig. 4 for *p*-wave levels is only an upper limit for D_1. A plot of the cumulative reduced neutron widths for *s*-wave resonances is shown in Fig. 5; a linear fit yields the strength function value $10^4S_0=0.17\pm 0.05$. A similar plot for *p*-wave resonances in Fig. 6 indicates a reduction of the observed strength above 700 eV because of decreasing experimental resolution. A linear fit to the resonances below 700 eV and application of Eq. (6) in the same energy region yield 10^4S_1 values of 3.0 ± 0.9 and 3.4 ± 1.0, respectively. The latter value is reported in Table II. The values of the average resonance parameters in the present work are consistent with values determined from previous measurements [8,13].

V. STATISTICAL TESTS

The distribution of the reduced neutron widths is expected to agree with the Porter-Thomas distribution [19]:

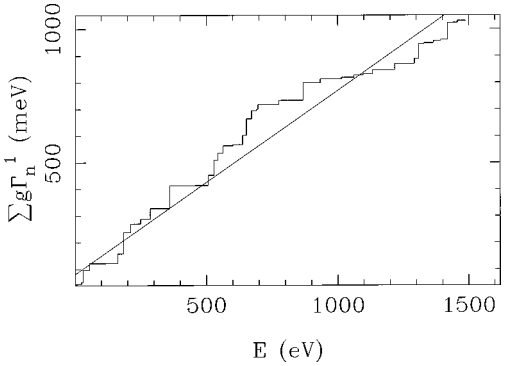

FIG. 6. Cumulative reduced neutron width for ^{117}Sn *p*-wave resonances with a linear fit below 700 eV (see discussion in Sec. V).

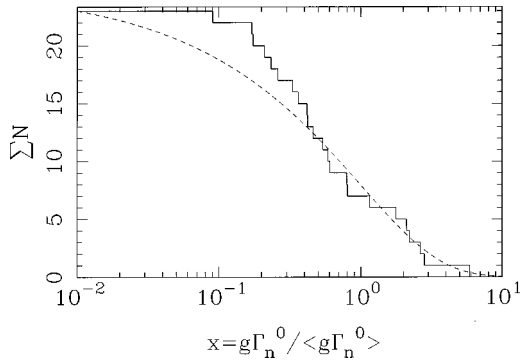

FIG. 7. Cumulative reduced width distributions for *s*-wave resonances compared to the Porter-Thomas distribution.

$$P(x)=\frac{e^{-x/2}}{\sqrt{2\pi x}}, \quad \text{where} \quad x=\frac{g\Gamma_{ni}^{l}}{\langle g\Gamma_{n}^{l}\rangle}. \tag{8}$$

Because of the limited number of resonances, the cumulative number of resonances is compared with the integrated distribution. Also, because states of smaller size are assumed to be missed, the integral of the distribution is shown from larger to smaller values. The corresponding cumulative reduced width distributions for *s* and *p* levels are compared with the integral of the Porter-Thomas distributions in Figs. 7 and 8. Such a comparison assumes the use of unbiased averaged $\langle g\Gamma_n^l\rangle$ values. Since a significant number of weak *p*-wave resonances are expected to be missed, we obtain an estimate for this average value indirectly. We used the experimental value of S_1, since the missing *p*-wave levels should be very weak and have relatively little effect on the strength function. However, the spacing is strongly affected by missing levels. Therefore we obtained the value of $D_1=27$ eV by scaling the value D_0 according to the $(2J+1)$ statistical factor: $D_1=(4/9)D_0$. From the strength function S_1 and the level spacing D_1 we obtained an unbiased $\langle g\Gamma_n^l\rangle$, which was used in the analysis. The normalization constant of the Porter-Thomas distribution—the total number of levels—was obtained by fitting the distribution to the histogram in the interval $0.7<x<7.0$ where the missing strength should be minimal. We note that the total number of levels under the full theoretical distribution is 8% larger than the number of levels in the theoretical distribution above the *y*

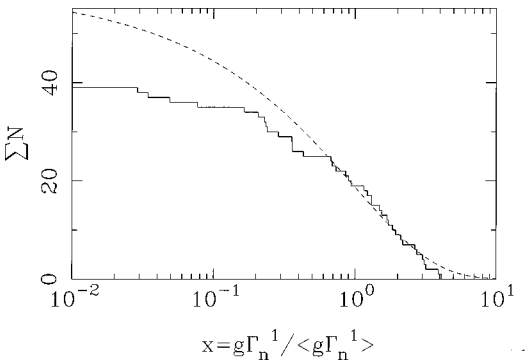

FIG. 8. Cumulative reduced width distributions for *p*-wave resonances compared to the Porter-Thomas distribution.

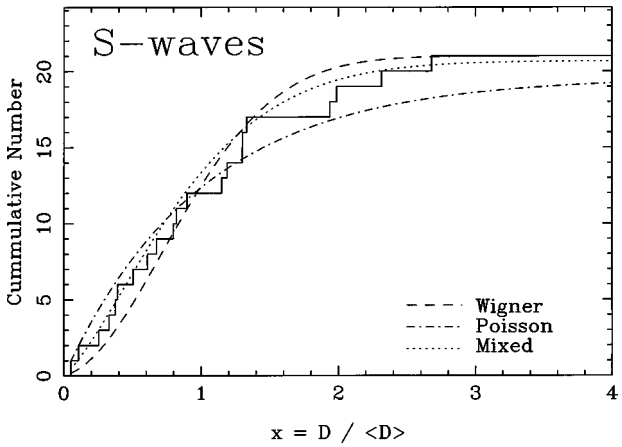

FIG. 9. Nearest-neighbor spacing distribution for the *s*-wave resonances up to 1.5 keV. The experimental distribution is compared with the Wigner distribution, the mixed two-sequence distribution (see text), and the Poisson distribution.

$=10^{-2}$ cut. Comparison with the histograms indicates that below 1.5 keV we miss about 8% of the *s*-wave and 35% of the *p*-wave resonances.

For a sequence of compound nuclear states with the same symmetry, the level spacings are expected to obey predictions of the Gaussian orthogonal ensemble (GOE) version of random matrix theory [20,21]. To a good approximation, the nearest-neighbor spacing distribution should obey the Wigner distribution

$$P(x)=\frac{\pi}{2}xe^{-\pi x^2/4}, \quad \text{where} \quad x=\frac{D_{li}}{\langle D_l\rangle}. \tag{9}$$

The other extreme, corresponding to no level repulsion or long-range correlations, is the Poisson distribution e^{-x}. In our experiment there are two spins for the *s*-wave resonances and three spins for the *p*-wave resonances. Therefore we expect to observe a linear combination of two *s*-wave GOE sequences and three *p*-wave GOE sequences. The relative weight is determined by the relative level densities. For this target nuclei with spin 1/2, the appropriate relative densities

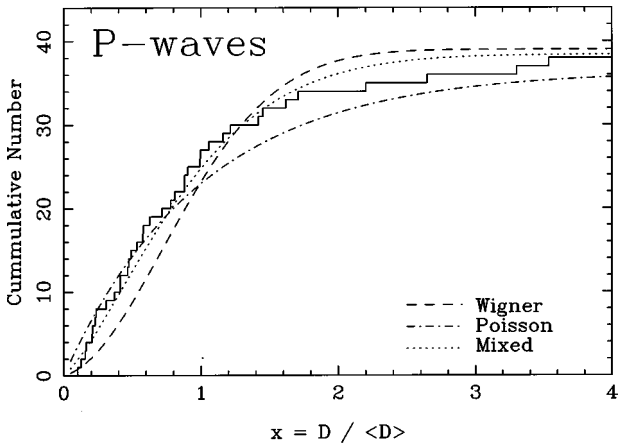

FIG. 10. Nearest-neighbor spacing distribution for the *p*-wave resonances up to 700 eV. The experimental distribution is compared with the Wigner distribution, the mixed three-sequence distribution (see text), and the Poisson distribution.

are 1/4 and 3/4 for the *s*-wave resonances and 1/9, 3/9, and 5/9 for the *p*-wave resonances. The numerical results are plotted in Figs. 9 and 10, for the Wigner distribution, the Poisson distribution, and the mixed Wigner distribution, along with the data. The distributions are normalized to the data such that they agree at infinity. Considering the fraction of levels missed the agreement with the GOE prediction is reasonable.

VI. SUMMARY

Neutron resonances were measured in ^{117}Sn from 1 eV to 1.5 keV using the radiative capture method. A total of 23 new resonances were identified in this energy region. We also have increased the accuracy in the determination of the resonance energies, most of the neutron widths, and the radiative widths for 12 of these resonances. The orbital angular momentum assignment was performed with a Bayesian analysis, and from this analysis 23 resonances are *s* wave and 39 *p* wave. The experiment below 1500 eV observed about 92% of the *s*-wave resonances expected in this region and about 65% for the *p*-wave resonances. From these data new values were determined for the average level spacings and strength functions for both *s*-wave and *p*-wave resonances. These results are consistent with past measurements. Knowledge of the ^{117}Sn resonance parameters permits the extraction of the rms weak matrix element from the observed parity nonconserving asymmetries [7], which will be published in a forthcoming paper.

ACKNOWLEDGMENTS

W. M. Snow, C. Keith, and D. Rich provided data on neutron flux measurements with ^{3}He, which was crucial in the analysis of these data. The authors would like to acknowledge the help of W. Scott Wilburn for discussions in the preparation of this paper. This work was supported in part by the U.S. Department of Energy, Office of High Energy and Nuclear Physics, under Grants Nos. DE-FG02-97-ER41042 and DE-FG02-97-ER41033, and by the U.S. Department of Energy, Office of Energy Research, under Contract No. W-7405-ENG-36.

[1] V. P. Alfimenkov, S. B. Borzakov, Vo Van Thuan, Yu. D. Mareev, L. B. Pikelner, A. S. Khrykin, and E. I. Sharapov, Nucl. Phys. **A398**, 93 (1983).
[2] J. D. Bowman, G. T. Garvey, Mikkel B. Johnson, and G. E. Mitchell, Annu. Rev. Nucl. Part. Sci. **43**, 829 (1993).
[3] V. V. Flambaum and G. F. Gribakin, Prog. Part. Nucl. Phys. **35**, 423 (1995).
[4] B. E. Crawford *et al.*, Phys. Rev. C **58**, 1225 (1998).
[5] S. L. Stephenson *et al.*, Phys. Rev. C **58**, 1236 (1998).
[6] J. D. Bowman, L. Y. Lowie, G. E. Mitchell, E. I. Sharapov, and Yi-Fen Yen, Phys. Rev. C **53**, 285 (1996).
[7] D. A. Smith *et al.*, Bull. Am. Phys. Soc. **42**, 1071 (1997).
[8] Yu. V. Adamchuk, V. S. Zenkevich, S. S. Moskalev, G. V. Muradyan, and Yu. G. Shchepkin, Sov. J. Nucl. Phys. **10**, 10 (1969).
[9] P. W. Lisowski, C. D. Bowman, G. J. Russell, and S. A. Wender, Nucl. Sci. Eng. **106**, 208 (1990).
[10] C. M. Frankle, J. D. Bowman, S. J. Seestrom, N. R. Roberson, and E. I. Sharapov, in *Time Reversal Invariance and Parity Violation in Neutron Resonances*, edited by C. R. Gould, J. D. Bowman, and Yu. P. Popov (World Scientific, Singapore, 1994), p. 204.
[11] J. D. Bowman, Y. Matsuda, Y.-F. Yen, and B. E. Crawford (unpublished).
[12] B. E. Crawford *et al.*, Phys. Rev. C **58**, 729 (1998).
[13] S. F. Mughabghab, M. Divadeenam, and N. E. Holden, *Neutron Cross Sections* (Academic Press, New York, 1981), Vol. 1, Pt. A.
[14] G. J. Russell, J. S. Gilmore, H. Robinson, G. L. Legate, A. Bridge, R. J. Sanchez, R. J. Brewton, R. Woods, and H. G. Hughes III, in *Proceedings of 10th International Collaboration of Advanced Neutron Sources*, edited by D. K. Hyer (Institute of Physics, Bristol, England, 1989), p. 483.
[15] D. Rich *et al.* (unpublished).
[16] S. L. Stephenson *et al.*, JINR Report E3-96-336 (JINR, Dubna, 1997), p. 171.
[17] L. M. Bollinger and G. E. Thomas, Phys. Rev. **171**, 1293 (1968).
[18] C. M. Frankle, E. I. Sharapov, J. A. Harvey, N. W. Hill, and L. W. Weston, Phys. Rev. C **50**, 2774 (1994).
[19] C. E. Porter and G. E. Thomas, Phys. Rev. **104**, 483 (1956).
[20] T. A. Brody, J. Flores, J. B. French, P. A. Mello, A. Pandey, and S. S. M. Wong, Rev. Mod. Phys. **53**, 385 (1981).
[21] T. A. Guhr, A. Müller-Groeling, and H. A. Weidenmüller, Phys. Rep. **299**, 189 (1998).